PHYSICAL REVIEW FLUIDS **2**, 034303 (2017)

Mechanics of gas-vapor bubbles

Yue Hao*
Atmosphere, Earth & Energy Division, Lawrence Livermore National Laboratory, Livermore, California 94550, USA

Yuhang Zhang† and Andrea Prosperetti‡
Department of Mechanical Engineering, Johns Hopkins University, Baltimore, Maryland 21218, USA
(Received 19 May 2016; published 23 March 2017)

Most bubbles contain a mixture of vapor and incondensible gases. While the limit cases of pure vapor and pure gas bubbles are well studied, much less is known about the more realistic case of a mixture. The bubble contents continuously change due to the combined effects of evaporation and condensation and of gas diffusion in the liquid and in the bubble. This paper presents a model for this situation and illustrates by means of examples several physical processes that can occur: a bubble undergoing a temporary pressure reduction, which makes the liquid temporarily superheated; a bubble subjected to a burst of sound; and a bubble continuously growing by rectified diffusion of heat in the presence of an incondensible gas.

DOI: 10.1103/PhysRevFluids.2.034303

I. INTRODUCTION

A bubble in a liquid usually contains a mixture of vapor and a permanent gas. There is a vast amount of literature dealing with the two limits in which one of the constituents predominates while the other one is essentially negligible (see, e.g., [1–7]). The physical basis for these approximations consists, on the one hand, in the relatively low vapor pressure of many liquids of practical interest at normal conditions and, on the other hand, in the ordinarily slight solubility and small diffusion coefficients of gases in liquids. To illustrate the former point it may be mentioned, for example, that the vapor pressure of water at 20 °C is only 2.3 kPa and therefore its effects in processes taking place at room temperature and normal pressure are small. Because of the small gas solubility in most liquids, in normal boiling, the gas flux into the bubble is orders of magnitude smaller than the vapor flux, which therefore controls the growth rate of the bubble.

There are several situations, however, in which the presence of gas in a bubble mostly filled with vapor or, conversely, of vapor in a bubble mostly filled with gas has important effects. In sonoluminescence, for example, the bubble expansion is huge, the collapse is very rapid, and vapor strongly affects the maximum temperature reached by the bubble content [8,9]. When a vapor bubble condenses, a small gas pocket full of the gas that diffused into the bubble during its growth is left behind. In flow cavitation, collapsing vapor bubbles leave behind many small gas bubbles produced by the same process (see, e.g., [3]). In both cases, these small gas bubbles may act as nucleation sites for the generation of new bubbles. Liquid degassing by boiling is another important process that relies on the combination of gas and vapor effects. When boiling takes place in an acoustic field, as in liquid degassing operations (see, e.g., [10,11]) or in enhanced boiling heat transfer (see, e.g., [12–15]), the presence of gas inside the bubbles strongly affects their behavior during the

*hao1@llnl.gov
†yzhan175@jhu.edu
‡Corresponding author: prosperetti@jhu.edu; also at Faculty of Science and Technology and J. M. Burgers Center for Fluid Dynamics, University of Twente, The Netherlands; present address: Department of Mechanical Engineering, University of Houston, Houston, TX 77204, USA.

compression phase of the pressure and gives rise to a faster growth by rectified diffusion of mass and heat, as will be seen below.

The present paper is devoted to the theoretical study of several situations that illustrate the strong effect of permanent gases on vapor bubbles. We consider the consequences of gas diffusion into a growing vapor bubble, the slowing down of the condensation process, and the enhanced growth by rectified diffusion. For the latter case, we investigate the formation of a gas-rich layer adjacent to the bubble surface, which decreases the flux of vapor toward the surface according to a well-known mechanism (see, e.g., [16]), which, however, has not been investigated in this particular context. The liquid we consider is water and the gas CO_2, whose large solubility brings out more clearly the effects that we illustrate. Furthermore, the closeness between the adiabatic index of water vapor and CO_2 permits some approximations that greatly simplify the mathematical model.

Literature on the general topic of gas-vapor bubbles is not plentiful. Nigmatulin and Khabeev [17] presented a mathematical model for the dynamics of spherical gas-vapor bubbles and illustrated a few of its predictions for a bubble abruptly exposed to a higher and a lower ambient pressure. Building on this work, Nigmatulin *et al.* [18] mostly focused on the oscillations and resonant behavior of gas-vapor bubbles. The latter topic was also addressed in a study by Nagiev and Khabeev [19]. In all of these studies the vapor mass flux at the liquid surface was calculated from the Hertz-Knudsen relation with a small accommodation coefficient equal to 0.04, which was a reported (but not universally accepted) value at the time. More recent results, from both molecular dynamics simulations and experiment, however, point to a significantly larger value, in fact, very close to 1 (see, e.g., [20–23]). This much larger value justifies the assumption of thermodynamic equilibrium used here, which has a considerable effect on the numerical results produced by the theory and is one of the reasons that justify the present study. Furthermore, the parameter space is large and the available examples do not illustrate a number of processes on which we focus here.

II. MATHEMATICAL MODEL

Throughout this paper, we will assume the bubble to remain spherical. For a stationary bubble, the validity of this assumption depends on the stability of the spherical shape. While a rather complete stability theory for gas bubbles is available (see, e.g., [6,9]), the matter has not been investigated for vapor bubbles specifically. Generally speaking, there are two destabilizing mechanisms. One is of kinematic nature and occurs during contraction of the bubble. The other one is dynamical, similar in nature to the Rayleigh-Taylor instability, and it occurs when compression of the bubble content slows down the inward motion of the bubble wall. Phenomena involving vapor bubbles are usually less violent than those encountered in acoustic cavitation and therefore one may expect the stability of the spherical shape to be less of an issue in this case. In any event, broadly speaking, stability prevails provided the velocity and acceleration of the interface are not too large.

We describe the radial motion of the bubble by the Rayleigh-Plesset equation corrected for slight compressibility effects of the liquid (see, e.g., [6,24]):

$$\left(1-\frac{\dot R}{c_L}\right)R\ddot R+\frac{3}{2}\left(1-\frac{\dot R}{3c_L}\right)\dot R^2=\frac{1}{\rho_L}\left(1+\frac{\dot R}{c_L}+\frac{R}{c_L}\frac{d}{dt}\right)\left(p-P-\frac{2\sigma}{R}-4\mu_L\frac{\dot R}{R}\right). \tag{1}$$

Here R is the bubble radius, p the pressure in the bubble, P the ambient pressure, σ the interfacial tension coefficient, and ρ_L, μ_L, and c_L the liquid density, viscosity, and speed of sound, respectively; overdots denote time differentiation and the subscripts L liquid quantities.

The radial dynamics of the bubble is strongly influenced by the way in which the internal pressure p depends on time. In order to determine this dependence accurately, it is necessary to consider the processes taking place in the bubble interior and at the liquid interface.

A. Bubble interior

The gas-vapor diffusion process is governed by the diffusion equation

$$\rho \frac{dC}{dt} = \nabla \cdot (\rho \mathcal{D} \nabla C) \tag{2}$$

or, more explicitly,

$$\frac{\partial C}{\partial t} + v \frac{\partial C}{\partial r} = \frac{1}{r^2 \rho} \frac{\partial}{\partial r} \left(r^2 \rho \mathcal{D} \frac{\partial C}{\partial r} \right). \tag{3}$$

Here $C = \rho_V / \rho$, with $\rho = \rho_V + \rho_G$ the total density of the gas-vapor mixture, is the vapor mass fraction, d/dt denotes the convective derivative with radial velocity v, $\mathcal{D}$ is the binary diffusion coefficient, and r is the radial distance from the bubble center. For perfect gases with molecular masses M_V and M_G we have

$$p_V = \frac{M_G C}{M_V + (M_G - M_V) C} p, \quad p_G = \frac{M_V (1 - C)}{M_V + (M_G - M_V) C} p, \tag{4}$$

with p the total pressure equal, by Dalton's law, to $p_V + p_G$; here and in the following the indices V and G refer to vapor and gas, respectively.

With the neglect of viscous dissipation, the enthalpy equation for a gas mixture is, in conservation form,

$$\frac{\partial}{\partial t} (\rho h - p) + \nabla \cdot (\rho h \mathbf{v}) = -\nabla \cdot \mathbf{q}, \tag{5}$$

in which h is the enthalpy, $\mathbf{v}$ the velocity field, and $\mathbf{q}$ the heat flux vector given by (see, e.g., [25,26])

$$\mathbf{q} = -k \nabla T - (c_{pV} - c_{pG}) T \rho \mathcal{D} \nabla C, \tag{6}$$

with k the thermal conductivity, c_p the specific heat at constant pressure, and T the absolute temperature. Pressure and temperature diffusion effects are important only in rather extreme cases (see, e.g., [27]) and have been disregarded. For a mixture of perfect gases we may write

$$\rho h - p = \frac{p}{\gamma_G - 1} + \Gamma p_V = \frac{p}{\gamma_V - 1} - \Gamma p_G, \tag{7}$$

where γ is the adiabatic index, p_V and p_G are the vapor and gas partial pressures, and

$$\Gamma = \frac{\gamma_G - \gamma_V}{(\gamma_G - 1)(\gamma_V - 1)}. \tag{8}$$

If the molecules of both vapor and gas consist of the same number of atoms and both behave as perfect gases, $\gamma_G = \gamma_V$ and $\Gamma = 0$. For the case of CO_2 and water vapor we have $\gamma_V \simeq 1.33$ and $\gamma_G \simeq 1.28$, so $\Gamma \simeq -0.54$.

Following earlier work [18,28,29], we assume that the bubble internal pressure is spatially uniform and only a function of time because of the very small inertia of the gas-vapor mixture. With this approximation and (7), upon integration, we find from (5) an expression for the velocity of the gas-vapor mixture in the bubble, namely,

$$\left(1 - \frac{\gamma_V - 1}{\gamma_V} \Gamma \frac{p_G}{p} \right) v = \frac{\gamma_V - 1}{\gamma_V p} \left[-q - \frac{r}{3} \frac{\dot{p}}{\gamma_V - 1} + \Gamma E_G \right], \tag{9}$$

with q the radial component of $\mathbf{q}$ and

$$E_G = \frac{1}{r^2} \int_0^r r^2 \frac{\partial p_G}{\partial t} dr. \tag{10}$$

In the numerical calculations we will proceed by assuming that the contribution of E_G is negligibly small. The effects of this approximation and its consistency will be demonstrated with a numerical

example in Fig. 14. For the time being we provide a crude estimate of the magnitude of the term E_G by approximating p_G by a polytropic relation $p_G/p_{G0} = (R_0/R)^{3\kappa}$, with p_{G0} and R_0 reference values and κ a polytropic index. In this way we find

$$\left|\frac{\Gamma E_G}{(r/3)\dot{p}/(\gamma_V - 1)}\right| \simeq 3\kappa \frac{|\gamma_G - \gamma_V|}{\gamma_G - 1}\left|\frac{\dot{R}}{\dot{p}}\right|\frac{p_G}{R} \simeq 3\kappa \frac{|\gamma_G - \gamma_V|}{\gamma_G - 1}\frac{\Delta R}{R}\frac{p_G}{\Delta p}, \tag{11}$$

with Δp and ΔR estimates of the internal pressure and radius changes, respectively. For $\Delta R \sim R$ and the preceding terms conservatively estimated to be a number of order 1, the ratio on the left-hand side of this relation is of the order of $p_G/\Delta p$. For a bubble containing mostly vapor, Δp is strongly dependent on the surface temperature, the effect of which is magnified by the large numerical value of the latent heat (about 3500 Pa/K for water near 100 ° C). The ratio may therefore be expected not to be large if the vapor is the dominant component of the bubble contents. Results for the converse case in which the gas is dominant can be found by switching the indices V and G in all the previous expressions, including the definition of E_G, and a similar conclusion would hold, particularly in the case of a cold liquid where the vapor density is low and the vapor pressure would change very little. When the amounts of gas and vapor are comparable, use of the simplification can be justified only when $\gamma_V \simeq \gamma_G$.

To determine the temperature field inside the bubble we use the gas enthalpy equation in nonconservation form, observing that the simultaneous use of the conservation and nonconservation forms of this equation is equivalent to the use of the equations of conservation of mass and enthalpy. For a two-component mixture of perfect gases the enthalpy equation takes the form

$$\rho\frac{dh}{dt} - \dot{p} = \boldsymbol{\nabla}\cdot[k\boldsymbol{\nabla}T + (c_{pV} - c_{pG})T\rho\mathcal{D}\boldsymbol{\nabla}C]. \tag{12}$$

Since $h = [c_{pV}C + c_{pG}(1 - C)]T$, we have

$$\begin{aligned}\rho dh &= \rho(c_G c_{pG} + c_V c_{pV})dT + \rho T(c_{pV} - c_{pG})dC = (\rho_G c_{pG} + \rho_V c_{pV})dT + \rho T(c_{pV} - c_{pG})dC \\ &= \left(\frac{\gamma_V}{\gamma_V - 1}p - \Gamma p_G\right)\frac{dT}{T} + \rho T(c_{pV} - c_{pG})dC \end{aligned} \tag{13}$$

and the enthalpy equation (12) becomes, after subtraction of some terms that reproduce the diffusion equation (2),

$$\frac{\gamma_V}{\gamma_V - 1}\left(1 - \frac{\gamma_V - 1}{\gamma_V}\Gamma\frac{p_G}{p}\right)\frac{p}{T}\frac{dT}{dt} = \dot{p} + \boldsymbol{\nabla}\cdot(k\boldsymbol{\nabla}T) + (c_{pV} - c_{pG})\rho\mathcal{D}\boldsymbol{\nabla}C\cdot\boldsymbol{\nabla}T. \tag{14}$$

B. Liquid

To complete the mathematical formulation it is also necessary to model the transport of heat and of mass in the liquid. For the former, unlike the previous treatment of the gas-vapor mixture, we disregard the effects of diffusion and use the energy equation for a pure substance

$$\frac{\partial T_L}{\partial t} + \frac{R^2}{r^2}\dot{R}\frac{\partial T_L}{\partial r} = D_L\nabla^2 T_L, \tag{15}$$

where D_L is the liquid thermal diffusivity. Since significant temperature nonuniformities are confined to the immediate neighborhood of the bubble wall, we disregard compressibility corrections to the incompressible velocity field $(R^2/r^2)\dot{R}$. In using this relation we implicitly neglect the very small difference between the liquid velocity at the interface and $\dot{R}$.

Gas diffusion in the liquid is described by

$$\frac{\partial \rho_g}{\partial t} + \frac{R^2}{r^2}\dot{R}\frac{\partial \rho_g}{\partial r} = \mathcal{D}_L\nabla^2\rho_g, \tag{16}$$

in which $\mathcal{D}_L$ is the mass diffusivity in the liquid. Here, since the liquid density is essentially constant irrespective of the amount of dissolved gas, it proves more convenient to use the dissolved-gas density ρ_g directly rather than the mass fraction as inside the bubble.

C. Interface conditions

At the bubble wall we impose the conservation of energy in the form

$$k_L \frac{\partial T_L}{\partial r}\bigg|_{r=R} + q(R,t) = L\dot{m}, \tag{17}$$

where L is the latent heat and $\dot{m}$ is the vapor mass flux (positive for evaporation)

$$\dot{m} = \rho_s C_s[\dot{R} - v(R,t)] + \rho\mathcal{D}\frac{\partial C}{\partial r}\bigg|_{r=R}, \tag{18}$$

where the subscript s denotes surface values, and the conservation of the gas mass

$$\rho_s(1 - C_s)[\dot{R} - v(R,t)] - \rho\mathcal{D}\frac{\partial C}{\partial r}\bigg|_{r=R} = \mathcal{D}_L \frac{\partial \rho_g}{\partial r}\bigg|_{r=R}. \tag{19}$$

In addition, we impose the continuity of temperature and Henry's law

$$\rho_g(R,t) = S\frac{p_G(R,t)}{H(T)}, \tag{20}$$

in which p_G is the gas partial pressure on the gas side of the interface and $S = \rho_L M_{CO_2}/M_L$, with M_{CO_2} and M_L the molecular masses of CO_2 and the liquid, respectively, is a conversion factor from moles to density; for the CO_2-water system considered here Henry's constant $H(T)$ is well represented by the correlation [30]

$$H(T) = \exp\left(-6.8346 + \frac{1.2817\times 10^4}{T} - \frac{3.7668\times 10^6}{T^2} + \frac{2.997\times 10^8}{T^3}\right), \tag{21}$$

where H and T are in units of MPa and K, respectively. The saturation vapor pressure is affected very little by the dissolved gas and we use the Clausius-Clapeyron equation in the form appropriate for a pure liquid-vapor system

$$\frac{dp_V}{dT_s} = \frac{L(T_s)\rho_{V,s}}{T_s}. \tag{22}$$

The boundary conditions of the problem couple many fields and their imposition requires some care. The first step is to obtain an equation for $\dot{p}$ from (17). For this purpose we substitute (18) for $\dot{m}$ into (17), with (9) used for v and (6) for q. Evaluating the result at the bubble surface, we have an equation for $\dot{p}$,

$$\begin{aligned}\frac{R}{3\gamma_V p}\alpha\dot{p} + \dot{R} = {} & \frac{k_L}{L\rho_s C_s}\frac{\partial T_L}{\partial r}\bigg|_{r=R} - \frac{\mathcal{D}}{C_s}\frac{\partial C}{\partial r}\bigg|_{r=R} + \left(\frac{\gamma_V - 1}{\gamma_V p}\alpha - \frac{1}{L\rho_s C_s}\right) \\ & \times\left[(c_{pV} - c_{pG})T_s\rho_s\mathcal{D}\frac{\partial C}{\partial r}\bigg|_{r=R} + k_G\frac{\partial T}{\partial r}\bigg|_{r=R}\right] + \frac{\gamma_V - 1}{\gamma_V p}\alpha E_G,\end{aligned} \tag{23}$$

where all the terms on the right-hand side are evaluated at $r = R$ and we have set $\alpha = [1 - \Gamma(\gamma_V - 1)p_G/\gamma_V p]^{-1}$ for simplicity of writing.

An equation for $\dot{T}_s$, the time derivative of the surface temperature, can also be found starting from (17): For this purpose we again use (18) to express $\dot{m}$ and eliminate $v - \dot{R}$ from (19) and q from (6)

to find

$$k_L \left.\frac{\partial T_L}{\partial r}\right|_{r=R} - k \left.\frac{\partial T}{\partial r}\right|_{r=R} = \left(\frac{L}{1-C_s} + (c_{pV} - c_{pG})T_s\right)\rho_s \mathcal{D} \left.\frac{\partial C}{\partial r}\right|_{r=R} + \frac{LC_s}{1-C_s}\mathcal{D}_L \left.\frac{\partial \rho_g}{\partial r}\right|_{r=R}. \tag{24}$$

Upon taking the time derivative following the interface this becomes an equation for $\dot{T}_s$. It may be preferable to take the time derivative after introducing the coordinate transformation, shown below in (28), that places the interface at $r/R = 1$.

For the vapor concentration at the bubble surface we use (4): Upon taking the time derivative, recalling that, at the bubble surface, p_V is determined by the surface temperature, we find an equation for $\dot{C}_s = (d/dt)C(R(t),t)$,

$$\dot{C}_s = M_G M_V \frac{\dot{p}_V p - p_V \dot{p}}{[M_G p + (M_V - M_G)p_V]^2}, \tag{25}$$

where

$$\dot{p}_V = \frac{\rho_V L}{T_s}\dot{T}_s \tag{26}$$

Alternatively, $\dot{p}_V$ can be calculated from (4) to find

$$\dot{p}_V = \frac{M_G}{M_V}\frac{p\dot{C} - C(1-\mu C)\dot{p}}{(1-\mu C)^2}. \tag{27}$$

Finally, the gas density on the liquid side of the interface is obtained from Henry's law (20).

III. NUMERICAL METHOD

The numerical method used to solve the energy and diffusion equations inside and outside the bubble is an extension of the one used in several earlier papers [24,31,32] to which the reader is referred for details. We introduce the variables

$$y = \frac{r}{R(t)}, \quad x = \frac{\ell}{\ell + r - R(t)}, \tag{28}$$

which map the intervals $0 \leqslant r \leqslant R(t)$ and $R(t) \leqslant r < \infty$ to $0 \leqslant y \leqslant 1$ and $1 \geqslant x > 0$, respectively. For the liquid energy and diffusion equations the length scale ℓ is taken to be a multiple B of the penetration length $\sqrt{D_L \tau}$,

$$\ell = B\sqrt{D_L \tau}, \tag{29}$$

where D_L is the appropriate diffusivity (for mass or heat) and τ a characteristic time scale; for the dimensionless constant B, we typically set $B = 10$. The temperature and concentration fields both inside and outside the bubble are then expanded in a truncated series of Chebyshev polynomials and the partial differential equations turned into a system of ordinary differential equations by collocation. In view of the zero-derivative condition at the bubble center and at infinity we only use the even polynomials. We found that 33 terms in all the expansions were sufficient to give converged results. The system of ordinary differential equations was solved by means the package LSODI. In order to validate the code we checked its performance in the limit of a bubble completely filled with vapor, finding results in agreement with the earlier ones of [24].

IV. RESULTS

The situation considered in this paper is characterized by too many parameters to lend itself to an exhaustive investigation and we will content ourselves with a few results illustrating the main phenomena. The first example, shown in Fig. 1, is that of a 1-mm-radius vapor bubble in water at

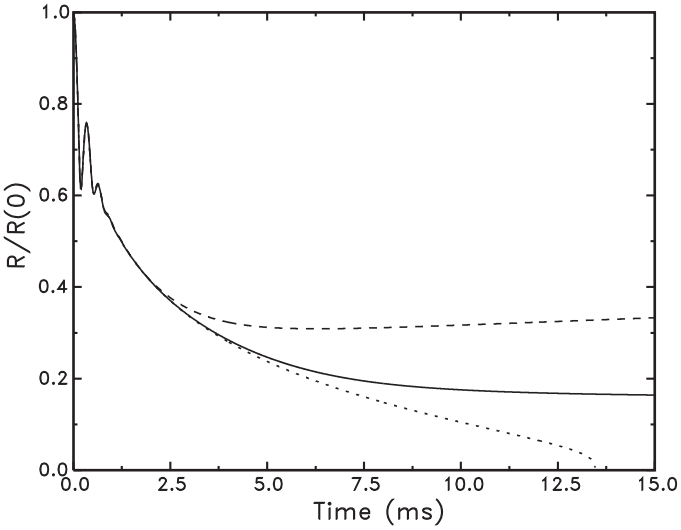

FIG. 1. A pure vapor bubble in water with no dissolved gas at 90 °C and 101.3 kPa ambient pressure quickly collapses (dotted line). The collapse is markedly slowed down if dissolved CO_2 is present in the liquid. The solid line is for water saturated with CO_2 at 100 °C and the dashed line for water saturated with CO_2 at 25 ° C. In this latter case the liquid is supersaturated at its temperature of 90 °C and, after the condensation of the vapor, the bubble begins to grow by gas diffusion.

90 °C under an ambient pressure of 101.3 kPa. We contrast the bubble behavior in water containing no dissolved gas (dotted line) with that in water saturated with CO_2 at 100 °C (solid line) and at 25 °C (dashed line). In the presence of dissolved gas, the collapse is markedly slowed down. Water saturated with CO_2 at 25 °C is actually supersaturated at 100 ° C, which causes the bubble to start slowly growing once the excess vapor initially present has condensed. In these three cases, at the initial time, the bubble contains only vapor with no CO_2. This initial condition is somewhat artificial when the liquid contains dissolved gas, but it permits a better comparison among the three situations.

The rapid and heavily damped oscillations visible at the beginning of the collapse in Fig. 1 can be understood by recalling the role of latent heat in providing the effective stiffness of a vapor bubble [7,24]. The initial rapid collapse deposits latent heat at the bubble surface, the temperature increases above saturation, and the pressure rises and causes a temporary reversal of the collapse. Upon expansion the bubble surface cools, the pressure falls, and a second rapid collapse follows. These oscillations are very rapidly damped and the bubble soon settles down to a quasiequilibrium situation characterized by a surface temperature fixed at the saturation level and, at this point, it starts its slow diffusive growth.

As a second example (Figs. 2–5), we consider a bubble that is subjected for a short time to a pressure low enough to render the liquid superheated. This is a simple model of a situation that may arise, for example, in flow boiling when bubbles are transported through a low-pressure region. These results are for a bubble with an initial radius $R(0) = 100\ \mu$m in water at $T_\infty = 100$ ° C. The water is saturated with CO_2 at 100 °C and $p_\infty = 101.3$ kPa, so $\rho_{g,\infty} = 0.488$ kg/m^3. The ambient pressure is 101.3 kPa, except for 5 ms $< t <$ 10 ms, when it falls to $P_{sat}(95\,^\circ\text{C}) = 0.8453$ kPa. The initial gas pressure in the bubble is 101.3 kPa, so the total bubble internal pressure is nearly twice as large as the ambient pressure. Thus, as the radius vs time graph of Fig. 2 shows, the bubble starts to grow already at $t = 0$ before the pressure is lowered. The rate of growth increases very rapidly when the pressure is lowered at $t = 5$ ms. During this growth the gas partial pressure decreases. The subsequent pressure recovery causes a rapid condensation of some vapor and an abrupt contraction of the radius. The rapid oscillations near $t = 10$ ms are similar to those visible at the initial stages

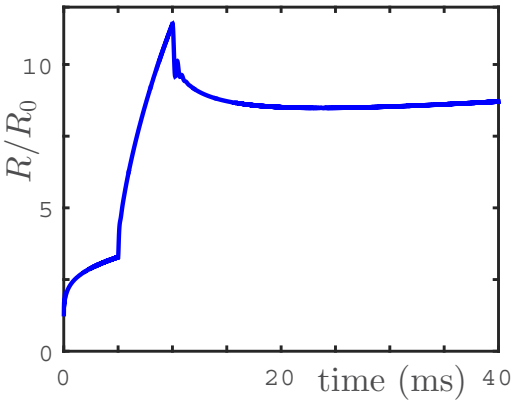

FIG. 2. Radius vs time of a gas-vapor bubble in CO_2-saturated water at 100 °C and 101.3 kPa. The liquid temperature is 100 °C and the ambient pressure 101.3 kPa except for 5 ms $< t <$ 10 ms, when it is reduced so that the liquid is superheated by 5 ° C. The initial bubble radius R_0 is 100 μm.

of the collapse in Fig. 1 of the previous example. The bubble contraction is arrested and eventually reversed by the combination of a vapor pressure increase, due to the temperature increase of the bubble surface caused by the release of latent heat, and the compression of the permanent gas. The radius reached during this stage is such that the total pressure in the bubble is close to the ambient pressure. Since this total pressure is the sum of the gas and vapor pressure, at the bubble surface the gas is now undersaturated and a concentration gradient exists that causes a slow growth of the bubble as gas diffuses into it from the liquid.

Figures 3–5 are, respectively, the gas mass, vapor mass, and overall gas mass fraction vs time in the bubble. The gas mass, shown in Fig. 3, increases during the entire process, while the vapor mass, shown in Fig. 4, rapidly decreases after repressurization. It is noteworthy that, during the period covered by the simulation, the total gas mass in the bubble increases by an order of magnitude. Even if the bubble were brought into contact with liquid cold enough to condense most of the vapor, its radius would still be more than twice as large as the initial value. This is the origin of the many small bubbles that are visible in subcooled boiling away from the hot region. The gas mass fraction, shown in Fig. 5, rapidly declines during the initial growth phases because the diffusion of heat is so much faster than that of mass that the bubble growth is almost entirely due to vapor generation.

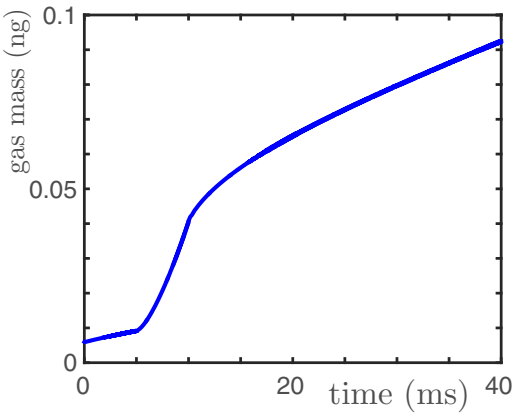

FIG. 3. Total gas mass in the bubble vs time for the case of Fig. 2.

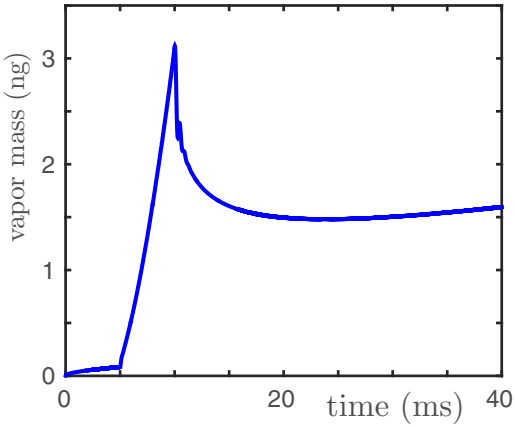

FIG. 4. Vapor mass in the bubble vs time for the case of Fig. 2.

Another interesting case is that of a bubble growing by rectified diffusion due to a burst of sound. This case is considered in Figs. 6 (bubble radius vs time), 7 (gas mass vs time), and 8 (vapor mass vs time). The initial bubble radius is 100 μm, the water temperature $T_\infty = 100\,^\circ$C, and the ambient static pressure $P_\infty = 101.3$ kPa. The liquid contains CO_2 corresponding to saturation at $25\,^\circ$C, $\rho_{g,\infty} = 1.52\,\mathrm{kg/m^3}$. Due to the low diffusivity of gases in liquids, this would be a typical scenario for water saturated with gas at the lower temperature and brought to a boil. A 1-kHz sound pulse, with a pressure amplitude of 30.39 kPa (0.3 atm), is applied between 0 and 30 ms ($0 < \omega t/2\pi < 30$).

Figure 6 shows the bubble rapidly growing by rectified diffusion of both heat and mass until, soon after it passes the resonant size, the sound is turned off. At this point the bubble executes a few strongly damped oscillations and starts shrinking due to vapor condensation even though, as is clear from Fig. 7, its gas content keeps growing.

As a final example, we compare the growth rate of an oscillating bubble containing only vapor with that of a bubble containing a gas-vapor mixture. The inhibiting effect of even a small amount of incondensible gas on vapor condensation under constant pressure conditions is well known (see, e.g., [26,33]). One might expect a similar phenomenon here, which would lead to a faster growth of the bubble by rectified diffusion because, for vapor to condense, it has to diffuse through a gas-rich boundary layer near the bubble surface while no such hindrance affects vapor generation at the interface.

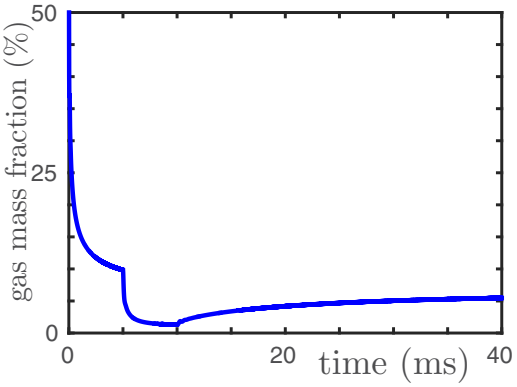

FIG. 5. Global gas mass fraction in the bubble vs time for the case of Fig. 2.

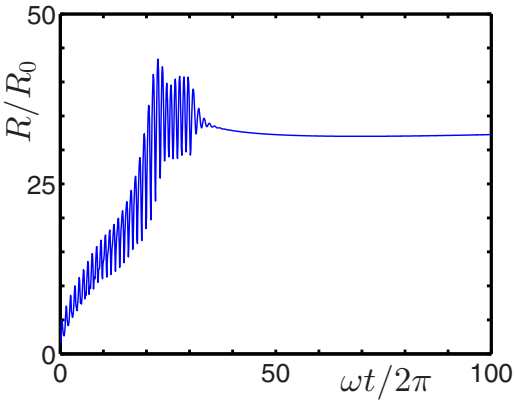

FIG. 6. Radius vs time of a gas-vapor bubble in water saturated with CO_2 at 25 ° C. The liquid temperature is 100 ° C. The ambient pressure is $101.3 \times (1 + 0.3 \cos \omega t)$ kPa for $0 \leqslant t < 30$ ms and 101.3 kPa thereafter; the sound frequency is $\omega t/2\pi = 1$ kHz. The initial bubble radius R_0 is 100 μm.

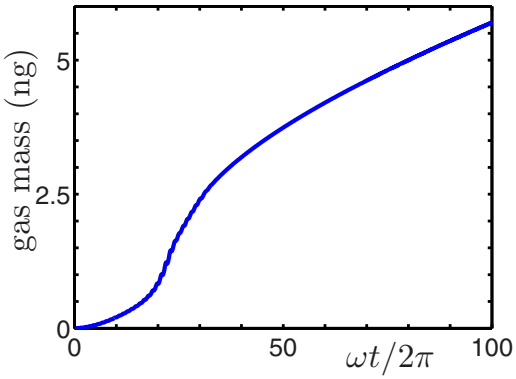

FIG. 7. Total gas mass in the bubble vs time for the case of Fig. 6. Since the liquid is saturated with CO_2 at 25 ° C, it is supersaturated at the temperature of 100 °C to which this figure refers, and gas diffuses into the bubble.

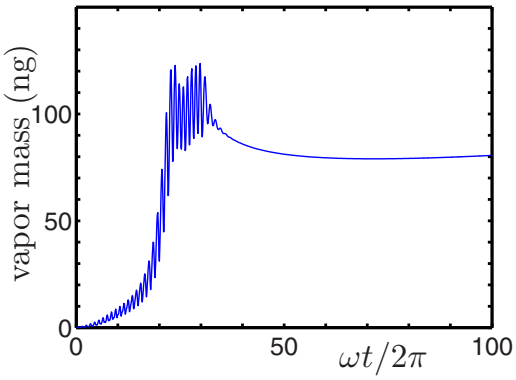

FIG. 8. Total vapor mass in the bubble vs time for the case of Fig. 6.

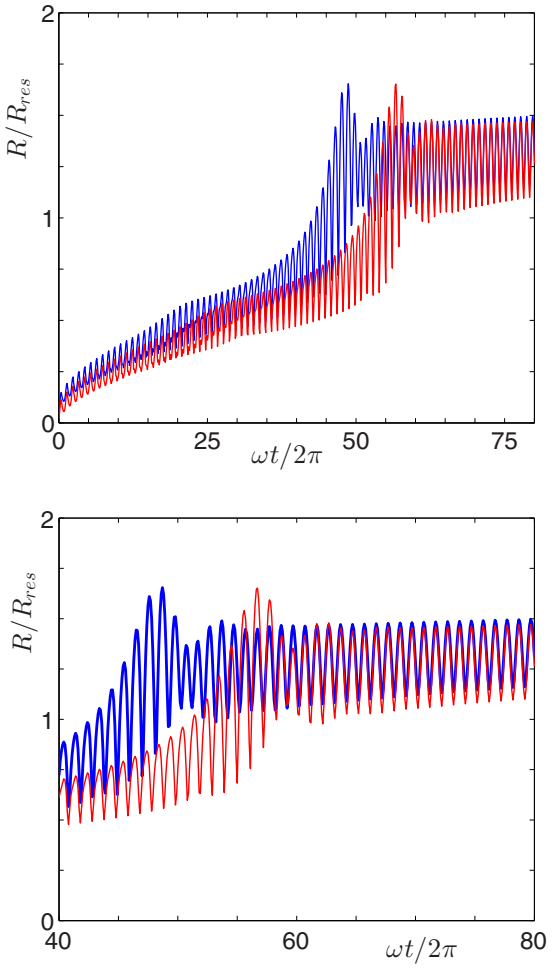

FIG. 9. Shown on top is the growth of a bubble containing CO_2 and water vapor (upper line) compared with that of a pure vapor bubble. The bottom panel shows an enlarged picture of the interval $40 \leqslant \omega t/2\pi \leqslant 60$, which contains the time interval in the course of which bubble executes large-amplitude oscillations. Here $T_\infty = 100\,^\circ$C, $P_\infty = 101.3$ kPa, the acoustic pressure is 30.4 kPa (0.3 atm), $R(0) = 0.2$ mm, $\omega/2\pi = 400$ Hz, and the bubble resonant radius is $R_{\rm res} = 7.27$ mm; the liquid is saturated with dissolved gas at 25 °C and is therefore supersaturated by a factor of approximately 16 at the liquid temperature used for the calculation; the initial vapor mass fraction inside the bubble is 25%.

That this is indeed the case is shown in Fig. 9, where the growth of a bubble containing CO_2 and water vapor (upper line) is compared with that of a pure vapor bubble (see also Fig. 10). Here $T_\infty = 100\,^\circ$C, $P_\infty = 101.3$ kPa, the acoustic pressure amplitude is $P_A = 30.4$ kPa, $R(0) = 200\,\mu$m, $R_{\rm res} = 7.27$ mm, and $\omega/2\pi = 400$ Hz. It is supposed here that the water was saturated with CO_2 at 25 °C (with a dissolved gas density of 1.52 kg/m^3) and was brought to 100 °C with no change in gas content rapidly enough for the dissolved gas not to equilibrate. The calculation is started with an initial gas mass of 5.9×10^{-11} kg, which corresponds to an initial vapor mass fraction of approximately 25%.

The mechanism underlying the increased growth rate is the accumulation of incondensible gas near the bubble wall, which takes place when vapor condensation begins at the start of the compression half-cycle: A concentration boundary layer builds up near the wall and offers a barrier

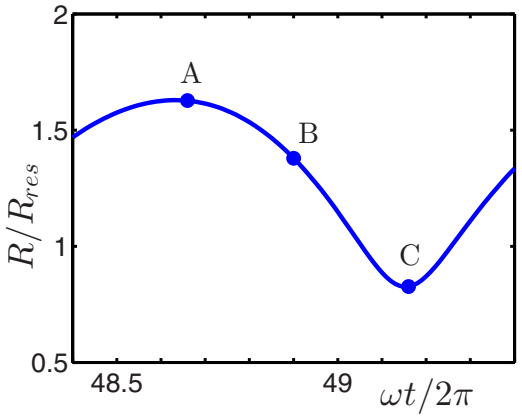

FIG. 10. Detail of Fig. 9 with circles marking the times corresponding to the mass fraction distributions shown in Fig. 11: A, $\omega t/2\pi = 48.66$; B, $\omega t/2\pi = 48.74$; and C, $\omega t/2\pi = 49.19$.

to further vapor condensation. The phenomenon is illustrated in Fig. 11 (where the lines are taken at the instants marked by circles in Fig. 10), which shows the gas mass fraction in the bubble at different times in the neighborhood of the interface. Near the point of maximum radius (point A) the gas concentration at the wall is small (note the logarithmic scale) but, as soon as the compression phase begins, the gas concentration near the interface grows significantly (point B) until it reaches a strong maximum when the radius reaches its minimum (point C). It should be noted that the average gas mass fraction in the bubble is less than 1%. The phenomenon is therefore quite sensitive to even small amounts of incondensible gases.

It is also interesting to consider the history of the bubble surface temperature and internal pressure for this case, which are shown in Figs. 12 and 13, respectively. Both quantities undergo very large excursions even though the oscillation amplitude of the bubble radius, while significant, is not very large. It is interesting to note, in both figures, the secondary peaks up to about $\omega t/2\pi = 30$. These structures are also present in the radius response of Fig. 9, although they are less clear there. Their origin lies in the fact that, as the bubble grows, the radius goes through values for which nonlinear

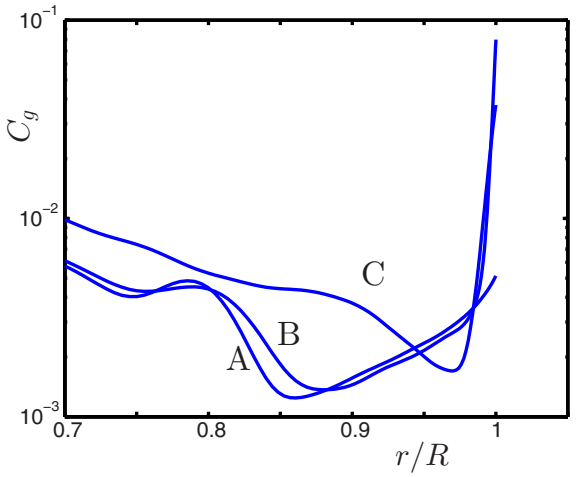

FIG. 11. Gas mass fraction distribution in the bubble at the three instants of time marked in Fig. 10. Notice the strong accumulation of gas near the interface when the vapor condenses during the compression cycle.

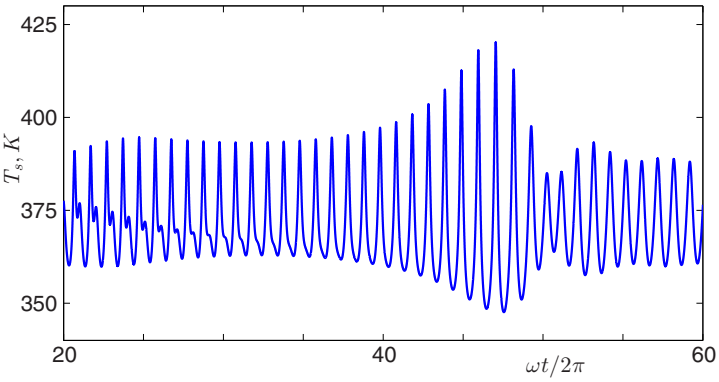

FIG. 12. Bubble surface temperature during a portion of the oscillations shown in Fig. 9.

resonances occur. For a gas bubble this would result in a prolonged time interval in the course of which a prominent second harmonic (in addition, of course, to others) is present. For a vapor bubble the mean radius grows so rapidly that only a few oscillations exhibit this nonlinear resonance.

To conclude, we illustrate for this case the effect of the neglect of the term E_G in (9) and (23). In principle, this term could be accounted for by integrating the equations neglecting it and then calculating E_G from its definition (10) using the approximate fields found in this way. Repeating the procedure would amount to an iterative solution of the problem. While this is likely a rather impractical algorithm, the procedure does afford us a way to check *a posteriori* the effect of the approximation and its consistency by stopping at the first step. We show in Fig. 14 a comparison between the volume-averaged velocity v calculated from (9) neglecting E_G (solid line) and including the first approximation found as just described (dots) for the example of Figs. 9 and 10. The top panel is for the initial portion of the calculation, while the bottom one focuses on the very-large-amplitude oscillations occurring for $40 \leqslant \omega t/2\pi \leqslant 50$. As can be seen, there is hardly any difference between the results with or without E_G, as could be expected on the basis of the considerations given after Eq. (10).

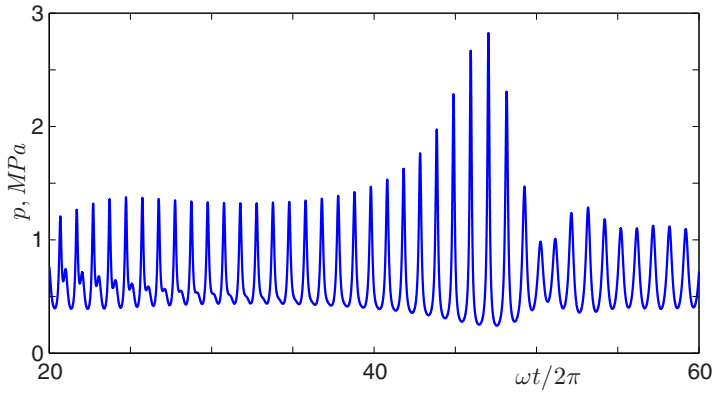

FIG. 13. Bubble internal pressure during a portion of the oscillations shown in Fig. 9.

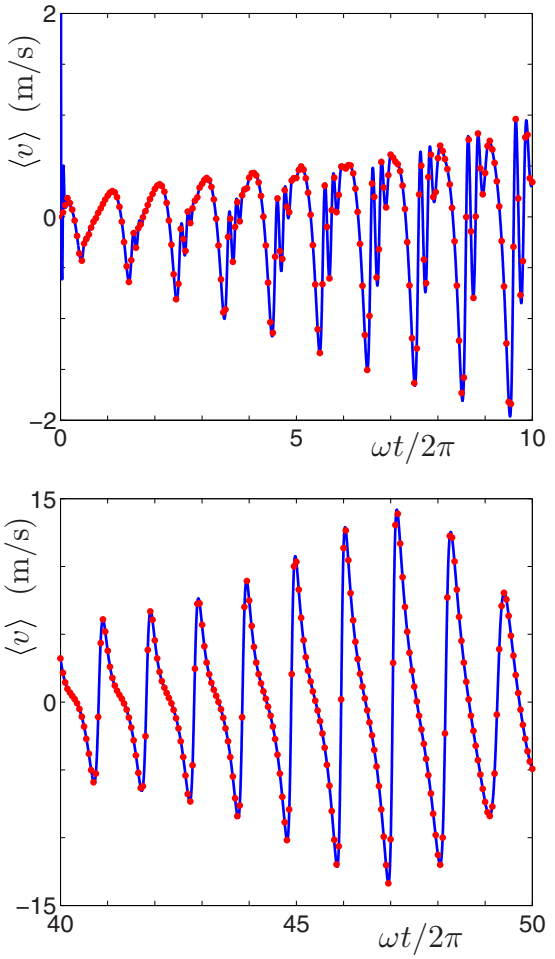

FIG. 14. Comparison of the vapor-gas velocity averaged over the bubble volume as computed from (9) without the E_G term (solid line) and corrected by including this term estimated as explained in the text.

V. CONCLUSION

The purpose of this paper is to illustrate a variety of phenomena that can take place when the liquid in which a vapor bubble is present contains a significant amount of dissolved gas. In order to bring out the effects more clearly we have considered the case of water with CO_2, which has a relatively high solubility in this liquid. In many practical cases boiling liquids are not degassed and failure to consider the diffusion of gas into and out of bubbles can lead to erroneous conclusions. An extreme case is a recent claim of persistent vapor bubbles in a cold liquid that are in fact bubbles full of gas that diffused into very short-lived vapor bubbles.

In our first example, a bubble collapses in water subcooled by 10 K at normal pressure. If only vapor is present the bubble quickly condenses in its entirety, but if CO_2 is dissolved in the liquid it diffuses into the bubble and markedly slows the collapse down. If the liquid is supersaturated with gas, the bubble first shrinks as the vapor condenses, but then starts to slowly grow as more gas diffuses into it. In a second example a small bubble in water with dissolved CO_2 at 101.3 kPa ambient pressure is briefly exposed to a lower pressure, which causes the liquid to become superheated by 5 K. The bubble quickly grows and, when the pressure recovers, it remains much larger than the initial

size due to the gas that has diffused into it during its growth. In another example the bubble is briefly exposed to an ultrasound pulse, which causes it to grow and again to persist due to the slow outward diffusion of the gas it acquired. The spatial nonuniformities of the fields inside the bubble can play an important role, e.g., in the process of rectified diffusion of heat when the bubble undergoes volume oscillations. The gas accumulates near the bubble surface and hinders the condensation of the vapor during the compression phase, thus increasing the growth rate of the bubble.

The mathematical model and numerical method used to generate these results have been described in some detail. The numerical solution is considerably simplified by the use of an approximation justified when the gas contains mostly vapor, or mostly gas, or when the ratios of the specific heats of vapor and gas are not too different. An extension to the general case is possible retaining the same general framework, although it would result in a more complex algorithm.

ACKNOWLEDGMENTS

Y.H.'s participation in this work was under the auspices of the U.S. Department of Energy by Lawrence Livermore National Laboratory under Contract No. DE-AC52-07NA27344. Y.Z. and A.P. gratefully acknowledge support from the NSF under Grant No. CBET1335965.

[1] M. S. Plesset and A. Prosperetti, Bubble dynamics and cavitation, Annu. Rev. Fluid Mech. **9**, 145 (1977).
[2] R. Nigmatulin, *Dynamics of Multiphase Media* (Hemisphere, Washington, DC, 1991).
[3] C. Brennen, *Cavitation and Bubble Dynamics* (Oxford University Press, Oxford, 1995).
[4] Z. Feng and L. Leal, Nonlinear bubble dynamics, Annu. Rev. Fluid Mech. **29**, 201 (1997).
[5] A. Prosperetti and Y. Hao, Modelling of spherical gas bubble oscillations and sonoluminescence, Philos. Trans. R. Soc. A **357**, 203 (1999).
[6] Y. Hao and A. Prosperetti, The effect of viscosity on the spherical stability of oscillating gas bubbles, Phys. Fluids **11**, 1309 (1999).
[7] A. Prosperetti, Vapor bubbles, Annu. Rev. Fluid Mech. **49**, 221 (2017).
[8] B. Storey and A. Szeri, Water vapour, sonoluminescence and sonochemistry, Proc. R. Soc. A **456**, 1685 (2000).
[9] M. P. Brenner, S. Hilgenfeldt, and D. Lohse, Single-bubble sonoluminescence, Rev. Mod. Phys. **74**, 425 (2002).
[10] J. Li, M. Tadashi, Y. Tayu, and Y. Fu, Application of ultrasonic treating to degassing of metal ingots, Mater. Lett. **62**, 4152 (2008).
[11] H. Puga, J. Barbosa, J. Gabriel, E. Seabra, S. Ribeiro, and M. Prokic, Evaluation of ultrasonic aluminium degassing by piezoelectric sensor, J. Mater. Process. Technol. **211**, 1026 (2011).
[12] K. A. Park and A. E. Bergles, Ultrasonic enhancement of saturated and subcooled boiling, Int. J. Heat Mass Transfer **31**, 664 (1988).
[13] Z. Douglas, T. R. Boziuk, M. K. Smith, and A. Glezer, Acoustically enhanced boiling heat transfer, Phys. Fluids **24**, 052105 (2012).
[14] S. Krishnan, S. K. Das, and D. Chatterjee, Physics of the interaction of ultrasonic excitation with nucleate boiling, ASME J. Heat Transfer **136**, 031501 (2014).
[15] R. E. Moehrle and J. N. Chung, Pool boiling heat transfer driven by an acoustic standing wave in terrestrial gravity and microgravity, Int. J. Heat Mass Transfer **93**, 322 (2016).
[16] L. C. Burmeister, *Convective Heat Transfer* (Wiley, New York, 1993).
[17] R. Nigmatulin and N. Khabeev, Dynamics of vapor-gas bubbles, Fluid Dyn. **11**, 867 (1976).
[18] R. Nigmatulin, N. Khabeev, and F. Nagiev, Dynamics, heat, and mass transfer of vapour-gas bubbles in a liquid, Int. J. Heat Mass Transfer **24**, 1033 (1981).

[19] F. B. Nagiev and N. S. Khabeev, Heat transfer and phase transition effects associated with oscillations of vapor-gas bubbles, Sov. Phys. Acoust. **25**, 148 (1979).
[20] P. Davidovits, D. R. Worsnop, J. T. Jayne, C. E. Kolb, P. Winkler, A. Vrtala, P. E. Wagner, M. Kulmala, K. E. J. Lehtinen, T. Vesala, and M. Mozurkewich, Mass accommodation coefficient of water vapor on liquid water, Geophys. Res. Lett. **31**, L22111 (2004).
[21] E. J. Davis, A history and state-of-the-art of accommodation coefficients, Atm. Res. **82**, 561 (2006).
[22] J. Julin, M. Shiraiwa, R. E. H. Miles, J. P. Reid, U. Poschl, and I. Riipinen, Mass accommodation of water: Bridging the gap between molecular dynamics simulations and kinetic condensation models, J. Phys. Chem. **117**, 410 (2013).
[23] J. Lee, T. Laoui, and R. Karnik, Nanofluidic transport governed by the liquid/vapour interface, Nat. Nanotech. **9**, 317 (2014).
[24] Y. Hao and A. Prosperetti, The dynamics of vapor bubbles in acoustic pressure fields, Phys. Fluids **11**, 2008 (1999).
[25] L. D. Landau and E. M. Lifshitz, *Fluid Mechanics*, 2nd ed. (Pergamon, New York, 1987).
[26] H. Baehr and K. Stephan, *Heat and Mass Transfer* (Springer, Berlin, 1998).
[27] B. Storey and A. Szeri, Mixture segregation within sonoluminescing bubbles, J. Fluid Mech. **396**, 203 (1999).
[28] R. Nigmatulin and N. Khabeev, Heat exchange between a gas bubble and a liquid, Fluid Dyn. **9**, 759 (1974).
[29] A. Prosperetti, The thermal behavior of oscillating gas bubbles, J. Fluid Mech. **222**, 587 (1991).
[30] J. J. Carroll, J. D. Slupsky, and A. E. Mather, The solubility of carbon dioxide in water at low pressure, J. Phys. Chem. Ref. Data **20**, 1201 (1991).
[31] Y. Hao and A. Prosperetti, The collapse of vapor bubbles in a spatially non-uniform flow, Int. J. Heat Mass Transfer **43**, 3539 (2000).
[32] Y. Hao, H. Oguz, and A. Prosperetti, Pressure-radiation forces on pulsating vapor bubbles, Phys. Fluids **13**, 1167 (2001).
[33] N. Khabeev, Diffusion effects in the oscillation of vapor-gas bubbles in a sound field, Int. J. Heat Mass Transfer **50**, 3556 (2007).